Late Oligocene midlatitude warming and temperate Early Miocene from alkenone-derived Sea Surface Temperature estimates

José Guitián[1,1] and Heather Stoll[1,1]

[1]ETH Zurich

November 30, 2022

Abstract

Large Antarctic ice volume changes characterized the middle to Late Oligocene and the first million years of climate evolution during the Miocene. However, the sea surface temperature (SST) evolution over this period remains poorly constrained, as only a few records from contrasting proxies are available. In this study, we present a long-term alkenone-derived SST record from sediments drilled by the Ocean Drilling Program (ODP) at Site 1168 in the west Tasmanian Sea spanning 29.8 Ma to 16.7 Ma. The SST record highlight that the long-term warming in the Late Oligocene linked to the end of the Middle Oligocene Glacial Interval can be recognized also at mid-to-high latitudes of the Southern Hemisphere. Warmer average temperatures (25.5°C) characterize the period from 24.6 to 22 Ma; average temperatures then decrease by 1 to 2°C into the Miocene and stabilize by 20.1 Ma. The reconstructed temperatures are highly variable in the warm Late Oligocene waters, and more stable and slightly colder in the Early to Middle Miocene. We confirm that this temperature trend is not an artefact of the latitudinal drift of the site, as the temperature anomaly relative to the modern water temperature at the paleolocation confirms the SST trends of the Oligocene. This is the first alkenone-derived record to reproduce the long-term Oligocene climate trend previously interpreted from the benthic δ18O, which recorded a warming and/or reduction in ice volume from the Middle Oligocene Glacial Interval through the latest Oligocene.

Evolution of Sea Surface Temperature in the Southern Mid-latitudes from Late Oligocene through Early Miocene

José Guitián[1] and Heather M Stoll[1]

[1]Geological Institute, ETH Zürich, Switzerland
Corresponding author: José Guitián (jose.paleocean@gmail.com)

Key Points:

- Alkenone-derived Sea Surface Temperatures from the Tasmanian Sea show cold conditions related with the MOGI.
- Despite the latitudinal drift of the site, the record confirms the long term warming during the Late Oligocene and a colder Early Miocene.
- This record highlights the different amplitudes of Late Oligocene warming obtained from different proxies and locations.

Abstract

Large Antarctic ice volume changes characterized the middle to Late Oligocene and the first million years of climate evolution during the Miocene. However, the sea surface temperature (SST) evolution over this period remains poorly constrained, as only a few records from contrasting proxies are available. In this study, we present a long-term alkenone-derived SST record from sediments drilled by the Ocean Drilling Program (ODP) at Site 1168 in the west Tasmanian Sea spanning 29.8 Ma to 16.7 Ma. The SST record highlight that the long-term warming in the Late Oligocene linked to the end of the Middle Oligocene Glacial Interval can be recognized also at mid-to-high latitudes of the Southern Hemisphere. Warmer average temperatures (25.5°C) characterize the period from 24.6 to 22 Ma; average temperatures then decrease by 1 to 2°C into the Miocene and stabilize by 20.1 Ma. The reconstructed temperatures are highly variable in the warm Late Oligocene waters, and more stable and slightly colder in the Early to Middle Miocene. We confirm that this temperature trend is not an artefact of the latitudinal drift of the site, as the temperature anomaly relative to the modern water temperature at the paleolocation confirms the SST trends of the Oligocene. This is the first alkenone-derived record to reproduce the long-term Oligocene climate trend previously interpreted from the benthic $\delta^{18}O$, which recorded a warming and/or reduction in ice volume from the Middle Oligocene Glacial Interval through the latest Oligocene.

1. Introduction

Suborbital resolution deep-sea benthic oxygen isotope records reveal large oscillations, at both orbital and multimillion-year timescales, over the Oligocene to Early Miocene time interval (De Vleeschouwer et al., 2017; Westerhold et al., 2020; Zachos et al., 2008) which are interpreted to reflect large variations in the Antarctic ice volume and temperature oscillations at the deep-water formation regions (Liebrand et al., 2017; Pekar and DeConto, 2006). The Oligocene presents a 2.5 myr long period of enriched $\delta^{18}O$ described as the Middle Oligocene Glacial Interval (MOGI) (Liebrand et al., 2017), followed by a long term shift towards lighter values from 26.5 Ma attributed to a Late Oligocene Warming (LOW) (Pekar et al., 2006; Villa and Persico, 2006). Some interpretations propose that the variation in benthic $\delta^{18}O$ signal is dominantly driven by ice volume, rather than deep-sea temperature (Liebrand et al., 2017). However, this deep-sea interpretation of climate has not yet been widely contrasted with long term and sea surface temperature (SST) records from mid to high latitude regions, which leaves the global SST reconstructions versus ice volume interpretation unclear.

The majority of available SST records spanning the Oligocene and Miocene are based on organic biomarkers, glycerol dialkyl glycerol tetraethers (GDGTs) TEX_{86} index and these present some paradoxes. GDGT-based estimates suggest similar absolute temperature at two tropical sites (O’Brien et al., 2020; Zhang et al., 2013) as at mid-to high latitude sites in the North and South Atlantic Ocean (O’Brien et al., 2020; Super et al., 2018), an absence of temperature gradients difficult to reconcile with climate models. While some of these records suggest long-term SST trends superimposed on higher frequency variability, GDGTs-derived temperatures from the Southern Ocean high latitude Site 1356 do not resolve multimillion year trends such as the MOGI or the Late Oligocene warming (Hartman et al., 2018) but do suggest high amplitude SST changes over orbital timescales starting at the Early Oligocene.

The few long-term SST records for the Oligocene to Early Miocene estimated from the long-chain alkenone unsaturation ratio ($U_{37}^{k\prime}$) are restricted to mid latitude sites in the North Atlantic, where they define punctuated excursions and multimillion-year variations coincident with the benthic isotope records (Guitián et al., 2019; Liu et al., 2018). However, these records are interrupted during part of the MOGI and during the Early Miocene, potentially underestimating the amplitude of its temperature change.

Therefore, additional SST reconstructions are required to explore the temperature variability at mid-to-high latitude sites, especially in the Southern Ocean, the region most proximal to the main polar ice cap in the Oligocene. To this end, this study presents a new alkenone-based SST record from $U_{37}^{k\prime}$ index over the Middle Oligocene to Early Miocene using sediments recovered from the West South Tasmanian Rise by the Ocean Drilling Program (ODP) at Site 1168 which had a estimated paleolatitude of 54°S by the middle Oligocene (Exon et al., 2001), ideal for providing a mid-latitude Southern Hemisphere view on surface ocean temperature. Our goal is to evaluate at this location whether there is a clear SST manifestation of the MOGI and LOW which were interpreted from global benthic $\delta^{18}O$. Although the relationship between ice volume and polar temperatures is complex (cite Bradshaw et al 2021, Evans et al 2021), recent models have proposed that large changes in the aerial coverage of Antarctic ice sheet do lead to coupled changes in SST around Antarctica which contribute to changing deep-sea temperature and benthic $\delta^{18}O$. Thus, although not providing a hard constraint on deep-water temperatures, our results can help assess the likelihood of an exclusively ice volume, vs combined ice volume and deep-sea temperature contribution to the amplitude of benthic $\delta^{18}O$ at this time.

The sediments of ODP 1168 preserve abundant biomarkers through the Oligocene and early Miocene. In this period, ODP 1168 transitions from carbonate-poor claystone to clay-bearing carbonate rich sediments related to deepening of the basin. Application of recent analytical techniques allow better separation of both C_{37} and C_{38} long chain alkenones (Longo et al., 2013) to identify alkenone indices that verify $U_{37}^{k\prime}$ -calculated SST trend despite the change in coastal proximity of the site where different alkenone producer populations may have different $U_{37}^{k\prime}$ to temperature calibrations (D'Andrea et al., 2016). The site location on the Tasmanian Rise was influenced by the gradual northward movement of the Australian plate, which widened the gateway between Australia and Antarctica and strengthened the exchange of water masses between the south Pacific and the Indian Ocean (Exon et al., 2002; Pfuhl and McCave, 2005; Pfuhl et al., 2004; Scher et al., 2015; Stickley et al., 2004b). We account for this latitudinal movement in the examination of temperature trends and gradients. Our SST record has an average 350 ky resolution, and although it exihibits high frequency variation potentially related to orbital cycles, coherent significant multi-million year scale trends in mean SST are evident. Biostratigraphic and magnetostratigraphic constraints on the age model allow us to compare our records with the existing SST reconstructions in the Southern Ocean to explore the evolution of temperature gradients, as well as with globally distributed SST estimates and high resolution benthic $\delta^{18}O$ from other sites.

2. Setting and sediments

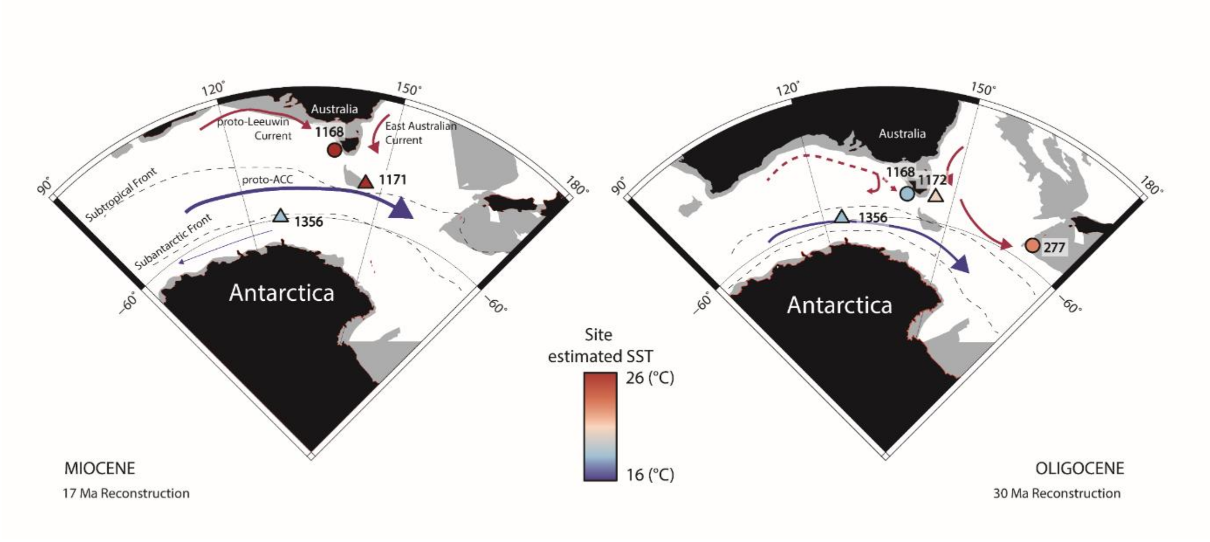

Figure 1. Reconstructed map of the study area with inferred surface ocean currents (red and blue solid and dashed lines) and convergent fronts (black dashed lines) (Salabarnada et al., 2018; Scher et al., 2015). Black fill denotes the paleo-location of the currently exposed continental area while the grey shading shows the continental rise. Site locations are shown with triangles and circles for GDGT-derived and alkenone-derived SST respectively, and are coloured as a function of the estimated paleotemperature at each timeslice after published SST estimates (Hartman et al., 2018; Houben et al., 2019; Leutert et al., 2020; Liu et al., 2009) (Table S1).

Site ODP 1168 is located in the offshore of the Australian plate at the western margin of Tasmania (Figure 1), at 43° 36.57’S and 139 144° 24.76’E, and 2463m water depth, drilled within a graben-developed basin with sediment accumulation since the latest Eocene (Exon et al., 2001). It is one of the few locations in mid paleolatitudes with relatively carbonate rich sequences for this time interval (Exon et al., 2001).

During the Late Eocene the area was within a system of migrating deltas and relatively restricted basins (Exon et al., 2001) which then led to a progressive deepening to 2.5 km by the end of the Miocene (Exon et al., 2001; Hill and Exon, 2004; Stickley et al., 2004b) as a consequence of the northward shift of the Australian continent. For the interval in our study, a recent synthesis of data including seismic stratigraphy suggest deepening from a paleodepth of about 700 m at 29 Ma to a depth of 1500 m for Site 1168 area by 21 Ma (Hochmuth et al., 2020). The deltaic coastline systems along the western Tasmanian continental margin and nearby isolated islands were most likely the source of material deposited at Site 1168 over the Early Oligocene (Exon et al., 2001; Hochmuth et al., 2020). Although carbonate content and preservation of biogenic calcite start to increase along the Early Oligocene, C/N ratios suggest that terrestrial organic matter input was predominant before 30.5 Ma (Exon et al., 2001). The lines of evidence suggest that, the gradual subsidence and increasing distance from the coast driven by the tectonic context in the area (Hill and Exon, 2004), resulted in a progressive change from dominance of shallow terrigenous sediments to pelagic carbonates during the Middle Oligocene (Exon et al., 2001). Therefore, the continuous stratigraphic sequence at Site ODP 1168 evolves from shallow-marine silty claystone in the latest Eocene and Early Oligocene, to clay-rich chalk and nannofossil ooze in the Miocene (Exon et al., 2001).

The paleoceanographic context is also paced by the progressive deepening of the Tasmanian Gateway, which played an important role in paleocirculation changes. The initial exchange of marine waters through the Gateway started during the Eocene (Stickley et al., 2004b). By 30 to 29 Ma, neodymium isotopes from fish teeth (recording bottomwater chemistry) at Site 1168 and the nearby but deeper Site 1172 had descended from typical Pacific signatures to values identical to the the Indian and Atlantic endmember, indicative of eastward flowing deep current from the Indian into the Pacific through an open gateway, inferred to indicate the onset of the Antarctic Circumpolar Current (ACC) (Scher et al., 2015).

For this study, 81 samples have been selected from Site 1168 Hole A in the 720 to 274 mbsf section of the recovered sequence. During our interval of focus, sediments are characterized by a gradual increase in %$CaCO_3$ content, from 10 % up to 70 %; particle size is dominantly silt and clay with sand content below 20 %, and Total Organic Carbon (TOC%) below 2% (Exon et al., 2001). This contrasts with older deposits, which feature higher TOC, larger grain size and lower carbonate content typical of nearshore conditions.

Today, Site 1168 is located north of the Polar Front (PF), Subtropical Front (STF) and the northern boundary of the ACC. Nevertheless, the site location has drifted in latitude following the Australian plate spread to the north away from Antarctic continent. Paleogeographic models estimate 7 degrees northward shift from 30 Ma to 15 Ma (Torsvik et al., 2012) from a paleolatitude of 55°S to a latitude of around 49°S. In addition, frontal position has also evolved since the Oligocene. The reconstructed paleoposition of the PF based on microfossil assemblages of diverse cores in the area is in the range from 60°S to 66°S (Scher et al., 2015). Although several reference frames of latitude drift have been reconstructed (O'Neill et al., 2005; Torsvik et al., 2008; Torsvik et al., 2012), in all of them Site 1168 appear to transit northward out of influence of the PF around 30 Ma and in no case later than 29.5 Ma.

The age model for Site 1168 has been in continuous revision since the first published shipboard reference based on biostratigraphy and magnetostratigraphic reversals (Pfuhl and McCave, 2003; Stickley et al., 2004a). Subsequent further refinements in nannofossil biostratigraphy provide a new detailed age model across the Oligocene to Miocene transition (Mcgonigal, 2004) which agrees well with previous chronology. In this study, we apply chronology updated to the Geological Time Scale from Gradstein et al. (2012) by Guitián et al. (2020) and modelled based on the original magnetostratigrahy and biostratigraphy (Stickley et al., 2004a) with resulting 95% confident intervals within 800kyr in the Oligocene and 400ky in the Miocene. Average sampling resolution is 290kyr. Although original magnetostratigraphy from 22 Ma to 21 Ma have uncertainties related to the weak magnetic signal, and there is some disagreement with biostratigraphic points (Mcgonigal, 2004; Stickley et al., 2004a) we consider this chronology sufficiently resolved for the long term and low-resolution scale of this study.

3. Methods

3.1 Organic extraction and biomarker analysis.

Preparation of organic samples was performed on a total lipid extract (TLE). From the samples selected to reach the target resolution, TLE was obtained from approximately 30g of freeze-dried disaggregated sediment extracted with an Accelerated Solvent Extractor 350. Solvent CH_2Cl_2/MeOH (9:1 v/v) in for four static cycles was used at 100°C. Once concentrated under purified N_2 stream, TLE was saponified with ~2 ml of a 0.5 M KOH in 95:5 MeOH:H_2O (optima grade). The neutral fraction was obtained using 0.5ml of Hexane shaking and pipetting out the saponified fraction three times. Silica gel column chromatography was then applied for further purification by eluting 4ml of Hexane, 4ml of CH_2Cl_2 and 4ml of MeOH for separation of the neutral fraction into a hydrocarbon fraction, a ketone fraction, including the long chain alkenones (LCA) and a polar fraction respectively.

Additional sample resolution was obtained from samples extracted at Utrecht University by Milestone Ethos X microwave system. CH_2Cl_2:MeOH 1:1 v/v was added to powdered and freeze-dried sample. This set of samples was not saponified, but only purified by column chromatography straight after the extraction splitting the TLE into an apolar, ketone and polar fraction using Hexane: CH_2Cl_2 (9:1 v/v), Hexane: CH_2Cl_2 (1:1 v/v) and CH_2Cl_2:MeOH (1:1 v/v).

Quantification of alkenones was performed by a Thermo Scientific Trace 1310 Gas Chromatograph (GC) equipped with a Flame Ionization Detector (FID) at ETH Zurich. The GC column was an Agilent VF – 200ms (60 m X 0.25 mm X 0.25 mm) coupled to a 5-m guard column from where 4 to 5 cm were trimmed before every sequence to avoid condensation or stack of non-eluting compounds. Helium at 2-ml/min was used as carrier gas flow. The GC oven was set at 60°C for one minute after injection and then ramped at 20°C/min to 255°C, 3°C/min to 300°C and finally 10°C/min to 320°C to be held 5 min. Several replicates and injection of an in-house alkenone standard (provided by G. O'Neil (Western Washington University) and C. M. Reddy (Woods Hole Oceanographic Institution) as well as n-alkane standards at every sequence were used to monitor the precision of the measurement and the performance of the instrument yielded a precision of 0.012 $U^{k\prime}_{37}$ units.

3.2 Alkenone unsaturation indices and Sea Surface Temperature estimations

We used the distribution and abundance of present long chain alkenones (LCA) biosynthesised by the haptophyte marine algae coccolithophores, to estimate previously defined carbon unsaturation indices. For temperature estimations, we applied the commonly used in palaeoceanography $U^{k\prime}_{37}$ ratio (Brassell et al., 1986; Prahl and Wakeham, 1987), based on the relative abundances of two compounds, $C_{37:2}$ and $C_{37:3}$, each with 37 carbon atoms and two or three carbon double bonds respectively:

$$U^{k\prime}_{37} = \frac{C_{37.2}\ \mathrm{Me}}{(C_{37.2}\ \mathrm{Me} + C_{37.3}\ \mathrm{Me})}$$

The 37-carbon methyl ketones, possess more double bonds with colder water temperatures. Alkenone-derived SST record was estimated based on the $U^{k\prime}_{37}$ unsaturation index using the BAYSPLINE calibration from Tierney and Tingley (2018). Although for high $U^{k\prime}_{37}$ in the BAYSPLINE calibration, uncertainties become larger, this calculation has the advantage of propagating the error through the SST calculations since errors are not uniform across the entire temperature range.

The $U^{k\prime}_{37}$ temperature calibrated with recent sediment samples and tested with culture studies for modern LCAs strains is widely assumed to yield accurate temperatures for earlier times in the Cenozoic. However, it has been proposed that non-thermal factors such as haptophyte algae assemblage composition or surface ocean productivity could affect the long chain alkenone distribution and abundances and therefore could bias the initial alkenone-derived SST reconstruction (Conte et al., 1998; Prahl et al., 2006) since $U^{k\prime}_{37}$ is calibrated to specific environment strains. Particularly for marginal ocean environments, it is proposed that environments with strongly contrasting salinity may host different alkenone-producing strains (Kaiser et al., 2017; Longo et al., 2016).

The analytical instrumentation applied in this study (mid-polarity stationary phase column, VF-200ms) identifies both C_{37} and C_{38} methyl and ethyl long chain alkenones with good resolution in the chromatogram (Longo et al., 2013). Therefore, when the C_{38} had sufficient concentration in our samples and were well resolved, we report $U^{k\prime}_{38Me}$ (Conte and Eglinton, 1993) derived from the distribution of the C_{38} methyl substitution:

$$U^{k\prime}_{38Me} = \frac{C_{38.2}\ \mathrm{Me}}{(C_{38.2}\ \mathrm{Me} + C_{38.3}\ \mathrm{Me})}$$

The index $U^{k\prime}_{38Me}$ has been previously suggested to be a more robust indicator of temperatures in settings which may be inhabited by diverse communities of haptophytes (Zheng et al., 2019) including members of Group II and Group I phylogenies as well as the typical marine Group III alkenone producers following the phylogenetic naming convention of Theroux et al. (2010). Today such mixtures of communities are most common in coastal or estuarine environments. These communities appear to have diverse intercepts between $U^{k\prime}_{37}$ and temperature (D'Andrea et al., 2016), potentially confounding paleotemperature estimates if the community composition is varying or is not represented by the same community as the calibration equation. In such settings the index $U^{k\prime}_{38Me}$ is expected to be more reliable because while C_{37} alkenones may be produced by Group I, II, and III, the relative production of methyl C_{38} is much greater in Group III marine alkenone producers, making its source and calibration therefore more restricted (Zheng et al., 2019).

To additionally explore potential algae distribution influencing the SST reconstruction, we computed further indices between C_{37} and C_{38} alkenones, since sensitivity of them to temperature is variable depending of the saline environment (Zheng et al., 2019). The ratio between them C_{37}/C_{38} (Rosell-Melé et al., 1994); relationship between all C_{37} and the ethyl C_{38} alkenones C_{37}/C_{38}Et; the ratio between the methyl and ethyl C_{38} alkenones C_{38}Me/C_{38}Et, and the specific compound RK2 ratio between di-unsaturated C_{37} methyl and C_{38} ethyl alkenones (RK2=$C_{37.2}$Me/$C_{38.2}$Et) (Zheng et al., 2019).

4. Results

4.1 Long Chain Alkenones abundance and distribution

The total of 53 samples extracted at ETH Zurich had diverse distribution of organic compound in the ketone fraction examined (Figure 2). The subset of samples which were not saponified but only purified with column chromatography present, as expected, a greater diversity of organic compounds, however the samples younger than 25 Ma, and some prior to 25 Ma, had well resolved and quantifiable LCA (Figure S1).

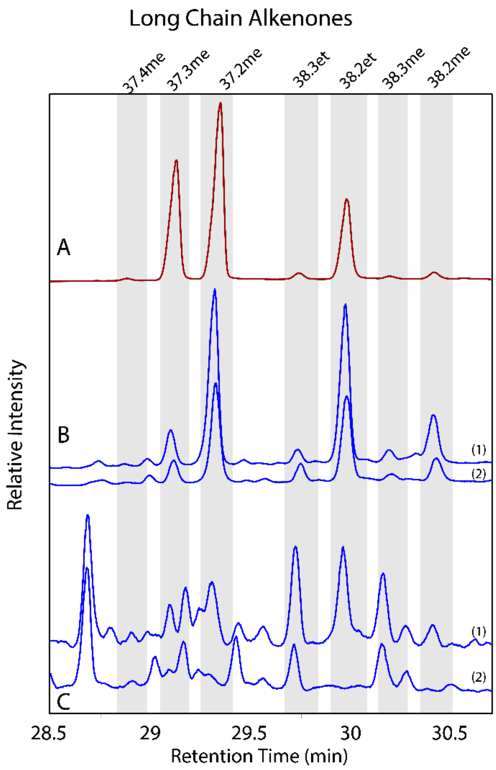

Figure 2. Illustrative chromatograms and long chain alkenones peaks of Site 1168 samples. (**a**) In-house alkenone standard. (**b**) Examples of well-resolved alkenones samples (1= 1168A-41X-4 W, 57.0-61.0 cm 22.1 Ma; 2= 1168A-37X-4 W, 52.0-58.0 cm 20.4 Ma). (**c**) Sample examples of unresolved chromatogram (1= 1168A-61X-1 W, 45.0-51.0 cm 27.9 Ma; 2= 1168A-75X-4 W, 130.0-136.0 cm 31 Ma.

With the methodology applied in this study, most of the samples older than 25.5 Ma present unresolved chromatograms in the retention time range corresponding to LCAs (Figure 3, Figure S1). These coeluting compounds complicate and in many cases preclude identification and quantification of chromatogram peak area. Only 8 samples in this segment featured chromatograms clean enough to quantify the various alkenones with confidence, including 3 where saponification was not performed.

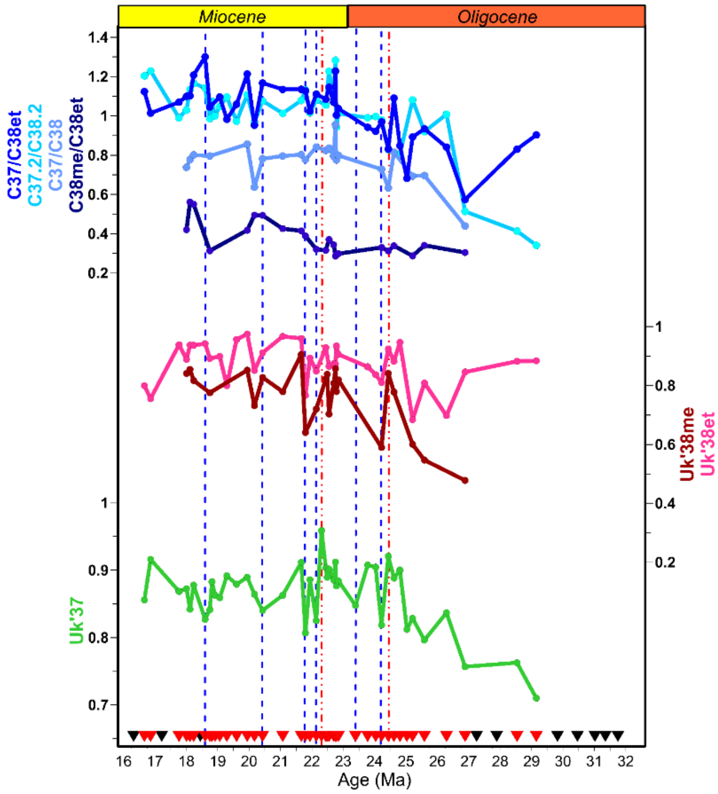

Figure 3. Biomarker results from ODP Site 1168. Vertical dashed lines after 25.5 Ma highlight lower and higher $U_{37}^{k\prime}$ than the mean variation with blue and red colours respectively. Bottom black and red triangles show samples with respectively unresolved and well resolved $C_{37.3}$ and $C_{37.2}$ compounds.

In contrast, the interval younger than 27 Ma is characterized by well resolved and identified long chain alkenones. In the ketone fraction, most of the C_{37} and C_{38} LCAs feature peaks with good shape and no coelution. From the chromatograms of this set of clean samples we are able to identify always two of the C_{37} ketones, the less abundant tri- and more abundant di-unsaturated alkenones. The C_{38} ketones, when all are present and resolved, have similar concentrations as the C_{37} being the $C_{38.2}$ ethyl ketone the most abundant. Some samples additionally presented C_{39} ethyl alkenones, however these were always below the detection limit for the analysis attempted in this study.

The ratio between all C_{37} and C_{38} alkenones gradually increases from 0.4 at 26.8 Ma to 0.9-1 by the Miocene (Figure 3). The compound specific ratio $C_{37.2}/C_{38.2}$ also gradually increases from 0.3 in the first identified sample at 29.2 Ma to 1.2 by the end of the record in the Miocene. The C_{37}/C_{38}Et ratio follows a similar trend and values as the total C_{37}/C_{38} and $C_{37.2}/C_{38.2}$, with the exception of the two oldest samples, which feature high ratios of C_{37}/C_{38}Et.

For the studied time interval, $U_{37}^{k\prime}$ ratio is presented and discussed for 43 samples from the most purified set, while the C_{38} unsaturation index $U_{38Me}^{k\prime}$ is resolved only in 24 samples. The oldest samples measured, at 29.2 Ma, feature the lowest $U_{37}^{k\prime}$ of 0.7. Subsequently $U_{37}^{k\prime}$ rises to 0.95 at 22.3 Ma, before stabilizing around 0.88 in the Early Miocene. The Index $U_{38Me}^{k\prime}$ follows a similar pattern despite the lower resolution. The highest correlation with $U_{37}^{k\prime}$ is found in the $U_{38Me}^{k\prime}$ index (r2=0.82) followed by the specific compound ratio $C_{37.2}/C_{38.2}$Et (r2=0.6) (Figure

S2). No relationship is found between obtained temperature related indices, $U^{k'}_{37}$ and $U^{k'}_{38Me}$, and the broad estimated concentration estimations of alkenone C_{37} and C_{38} applied in this work (Figure S2, S3).

4.2 Late Oligocene to Early Miocene SST estimations

BAYSPLINE-derived SST using the $U^{k'}_{37}$ index range from 19°C to 29°C in the Late Oligocene to Early Miocene at ODP Site 1168 (Figure 4). Data show long-term warming in the Late Oligocene of 5°C, from 29 Ma (~21°C) to 24.7 Ma (~26°C) coincident with the Late Oligocene Warming originally identified in benthic isotope records (Pälike et al., 2006; Pekar et al., 2006). Average temperatures are stable around 25°C through the Oligocene to Miocene transition to later cool down 2°C into the Miocene from 22.6 to 21.1 Ma. Later on, stable temperatures, around 24.5°C characterize the record.

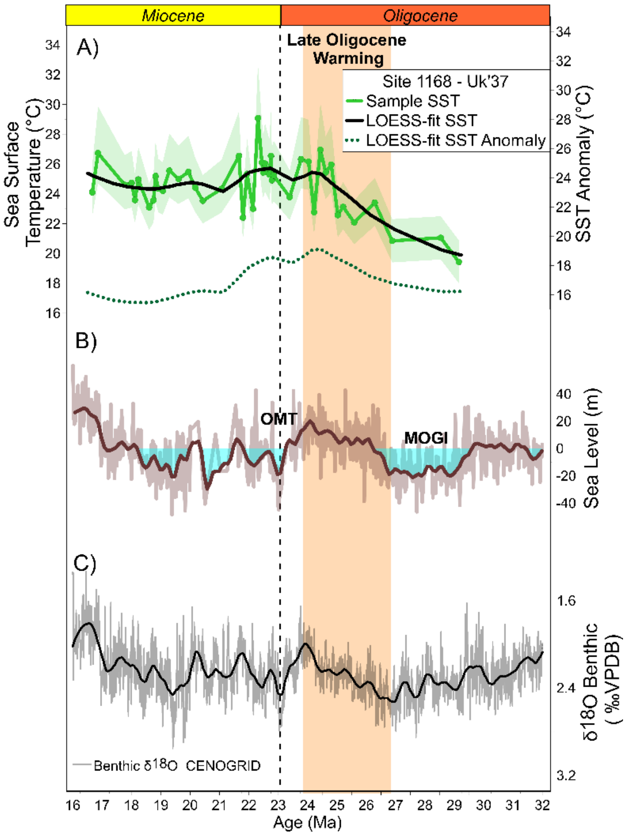

Figure 4. SST reconstruction for ODP Site 1168 and global climatic signatures. (**a**) Mean SST Bayspline reconstruction with 1-sigma CI (green). Black line describe fitted data with LOESS model. Dashed line shows SST anomaly reconstruction. (**b**) Sea level reconstructions from Miller et al. (2020). Filled blue colour are intervals with negative sea level. (**c**) Benthic foraminifer oxygen isotope reference (Westerhold et al., 2020). Vertical orange band shows the interval identified as the Late Oligocene Warming.

5. Discussion

5.1 Confirmation of marine-dominated SST signal with LCA

Because the environment of sediment deposition at ODP 1168 went through significant changes over the 12 million year interval explored here, before interpreting the SST signal we assess the potential effect of changing sedimentary environment on the biomarker signal. Furthermore, while alkenone SST is a widely applied proxy and a marine core top calibration is widely established (Conte et al., 2006; Müller et al., 1998; Tierney and Tingley, 2018), recent studies have revealed that diverse phylogenetic lineages characterize alkenone production in freshwater, brackish, and marine environments (Theroux et al., 2010). Cntrasting lipid distributions in these lineages may contribute to varying $U_{37}^{k\prime}$ index at the same temperature among the different lineages (D'Andrea et al., 2016). Today, some marine environments allow the coincidence of both open ocean alkenone producers and the Group II alkenone producers typical in estuarine environments (Longo et al., 2013; Zheng et al., 2019). Because ODP 1168 was located near the coast in the early Oligocene, we therefore use a wide array of lipid indices to evaluate whether that the $U_{37}^{k\prime}$ index and marine calibration are yielding appropriate temperature estimates.

The lowermost sediments analyzed here are characterized by a greater diversity and complexity of biomarkers and coincide with the high TOC % (>1%wt) and low $CaCO_3$ (<10%) characteristic of the marginal and deltaic marine settings in the Early Oligocene at the location (Exon et al. (2001); Figure S1). The diversity of organic compounds might be affected by changes in diagenetic reactions as the site gradually subsides into deeper, more oxygenated waters, potentially moving out of the oxygen minimum zone by 29 Ma (Exon et al., 2001; Hill and Exon, 2004; Hochmuth et al., 2020). The good LCAs signal afterwards appear to be related to the simultaneous gradual opening of the restricted basin leading to an increase in ventilation and oxygenation of the regional water column following the invigoration of currents through the opening gateway. If sediments were subject to different oxygen exposure time, this could affect temperature estimates if more unsaturated compounds were easier to degrade as initially proposed (Brassell, 1993; Rechka and Maxwell, 1988). However, other results show less conclusive selectivity of degradation (i.e. Gong and Hollander, 1999; Grimalt et al., 2000) and affirm there is no consistent evidence of selective degradation of diunstaurated versus tri-unsaturated alkenones at depleted oxygen waters or sediments not affecting the ratio between C_{37} alkenones in sediments nor while settling in the water column (Grimalt et al., 2000). Thus we conclude that the temperature estimation is not biased by evolution in the sedimentary conditions at the site.

Several lines of evidence suggest that SST evolution inferred from our $U_{37}^{k\prime}$ is not significantly altered by changes in the contribution of non-marine alkenone producers. The main coccolithophore skeleton preserved at Site 1168 sediments are the reticulofenestrids group (Guitián et al., 2020; Wei et al., 2003). They are known to be the ancestors of the modern open ocean alkenone producers, *E. huxleyi* and *G. oceanica*, (Marlowe et al., 1990; Volkman et al., 1980; Young, 1998) included in Group III (Theroux et al., 2010) and therefore SST is interpreted from modern core top calibrations. However, the modern estuarine Group II alkenone-producers do not make mineralized skeletons so lipid indicators must be used to assess their potential contribution. Since algae from brackish to saline environments generally do not generate as C_{38} methyl alkenones as the ocean water ones (Lopez et al., 2005; Zheng et al., 2019; Zheng et al., 2017), Zheng et al. (2019) suggested that temperature reconstructions from the ratio $U_{38Me}^{k\prime}$ will provide robust estimations which are free from artefacts of changing relative abundance of Group II and Group III haptophytes algae. We present unsaturation indices from the C_{38} LCAs (Figure 3; Figure S1), however, $U_{38Me}^{k\prime}$ could be calculated for only

24 samples. We document that when large changes in $U^{k'}_{37}$ are found, (i.e. from 29 to 24 Ma), $U^{k'}_{38Me}$ covary with $U^{k'}_{37}$, (r2=0.82). This supports interpretation of the $U^{k'}_{37}$ as caused by SST variations, not changes in the alkenone-producing community.

One additional evidence of the marine origin of the $U^{k'}_{37}$ involved lipids is the covariance obtained from the $C_{37.2}$Me and $C_{38.2}$Et relationship, RK2 index (Zheng et al., 2019) (Figure 3). Both LCAs are produced among different species groups but their ratio is more sensitive to temperature in the open marine environments strains (Zheng et al., 2019). In our dataset, the RK2 is positively correlated with the temperature related indices, which suggests the open water marine, rather than estuarine, source of LCAs (r2: 0.64 $U^{k'}_{37}$; r2=0.51 $U^{k'}_{38Me}$) (Figure S2). This evidence leads us to interpret the long-term trend in $U^{k'}_{37}$ as most likely derived from ocean water algae assemblage and the temperature estimates are not biased due to influence of other alkenone producing families such as those found in modern coastal or low saline environments.

Due to the shallow position of ODP Site 1168, sedimentation likely support little horizontal drift of the organic compounds as settling down from the surface. As the surface paleo circulation followed the west-east direction with the Proto – Leeuwin current, parallel to the Australian Margin (Stickley et al., 2004b), suggests that low potential for compounds to have been produced in areas with large differences in temperatures.

5.2 Site 1168 Sea Surface Temperature Trends

5.2.1 Sensitivity of temperature trends to latitudinal movement and setting

Aliasing of high frequency orbital variability in SST, as well as the latitudinal movement of the site, may affect the long-term temperature trends observed at this site. To reduce the influence of high frequency variability on long-term SST variation, we also present a smooth of the long-term trend by applying a local polynomial regression model (LOESS) (Figure 4). The smoothed trend shows a long term warming of 5°C from the Middle to the Late Oligocene, reaches a maximum around 26°C during the transition from the Oligocene to the Miocene, and then cools down to stabilize at 24.5°C until the end of the record at 16.7 Ma.

Since the South Tasmanian margin has drifted northwards from paleolatitude of 55°S to 48°S over the Oligocene to Miocene interval sampled here, we follow the approach described by Herbert et al. (2016) to distinguish the component of SST change due to regional climate variation, from that due to the migration of the site to warmer latitudes. We calculate a temperature anomaly as the difference between the smoothed LOESS-fit temperatures for ODP Site 1168 (Figure 4) and the modern mean annual temperature (Locarnini et al., 2013) at the backtracked paleolatitude and longitude of Site 1168 position at the age of each $U^{k'}_{37}$ sample. Paleogeography is reconstructed according to (van Hinsbergen et al., 2015) which is based on the paleo magnetic reference frame of (Torsvik et al., 2012). The estimated anomaly reaffirms that there is a regional warming in the Late Oligocene by 4°, which is not an artefact of the migration of the site. The calculated anomaly also indicates a relatively colder Early Miocene. Because the paleolatitude range of Site 1168 spans the modern Polar Front (PF) region of steepened temperature gradients, whereas the micropaleontological assemblages at multiple sites indicate that the PF remained poleward of Site 1168 in the Oligocene-Miocene (Scher et al., 2015), the corrected temperature anomaly may underestimate the actual regional warming through the Oligocene to Early Miocene.

We propose that the SST trends obtained from Site 1168 between 29.2 Ma and 16.7 Ma are representative of regional warming/cooling because they postdate the reorganization of ocean currents accompanying basin opening and the northward shift of the Tasmanian margin (Stickley et al., 2004b). Neodymium isotopes on fossil fish teeth at Site 1168 confirm the eastward flow from the Pacific Ocean in intermediate depths following the northward migration of the gateway into the influence of the westerly wind achieved by 29 Ma (Scher et al., 2015). Paleobathymetry reconstructions further support the existence of an important shallow to intermediate water exchange already by 30 Ma (Hochmuth et al., 2020).

5.2.2 Late Oligocene – Early Miocene SST trends

Our Southern Hemisphere SST record commences a few million years after the abrupt decrease in deep ocean temperature and increase in Antarctic ice volume recorded by benthic $\delta^{18}O$ across the EOT (Figure 4). Our record begins within the MOGI, defined by oxygen isotope records and a 2-myr lowstand sea level (Liebrand et al., 2017; Miller et al., 2020), and we record relatively low SST. The most prominent feature of our SST record is the warming of up to 5.5°C in the LOESS-smoothed record represented by 4°C increase in the calculated SST anomaly, from ca 29 to 24.5 Ma. This long term warming is simultaneous, within the age uncertainty, with the negative long term benthic $\delta^{18}O$ shift starting at 27 Ma (De Vleeschouwer et al., 2017; Zachos et al., 2008) described as the Late Oligocene Warming (Pekar et al., 2006; Villa and Persico, 2006).

The transient cooling and ice build-up reflected in a large positive benthic excursion at the Oligocene Miocene boundary was likely not sampled by the resolution of this study. Light reflectivity (L*) generated by the shipboard expedition (Exon et al., 2001), does present a significant turning point at the surrounding depths of the expected OMT applying the age model from Guitián et al. (2020) used in this study (Figure S4), coincident with changes in rates of sediment accumulation, where SST is not sampled. These data suggest that our smoothed trends over the Oligocene Miocene transition do omit orbital events of shorter duration..

Our estimates of temperature anomaly suggest an average colder Early Miocene than latest Oligocene, with a 1-myr. cooling from 25.5°C starting at 22.7 Ma, to stabilization of absolute temperatures around 24.4°C thereafter until 16.7 Ma (Figure 4). Those estimates are in agreement with relatively lower sea level reconstructions in the Early Miocene, and more positive benthic $\delta^{18}O$, although benthic records feature higher variability than Miocene SSTs at ODP 1168.

During the Early Oligocene, the cool SST we have reconstructed at Site 1168 are largely coherent with the available SST estimates from nearby sites in the Southern Ocean and expected post-EOT latitudinal temperature gradients (Kennedy-Asser et al., 2020) (Figure 1). In the Atlantic sector of the Southern Ocean at ODP Site 1090, with estimated paleolatitude 7° equatorward of Site 1168, average alkenone-derived temperatures are 3.1°C warmer than Site 1168 in the Early Oligocene (27.7 to 33 Ma)(Liu et al., 2009), in agreement with the modelled latitudinal gradient for post EOT times (Kennedy-Asser et al., 2020). The average 2.3°C warmer GDGTs-derived temperatures at nearby Site 1172 at 30 Ma (Houben et al., 2019) could reflect a greater influence of warm poleward currents at ODP 1172 or effects of different proxy calibration or habitat (Figure 1; Table S1). Compared to temperatures estimated at a pre-EOT 33 Ma time slice east of the Tasmanian Gateway at DSDP 277 (Liu et al., 2009), our oldest temperature estimates are only 3.1°C and 4.7°C colder than alkenone and GDGT-derived reconstructed temperatures, respectively. The most surprising comparison is that our early Oligocene temperatures are considerably warmer than those obtained at ODP Site 511 (31-32.5 Ma), east of the Drake Passage in the South Atlantic, which estimated 9°C alkenone -derived and 15°C GDGTs-derived temperatures (Houben et al., 2019; Liu et al., 2009).

Our mid Miocene (16.7 Ma) estimate of 24°C SST at Site 1168 is consistent with recent TEX_{86} reconstructions at Site 1171, located only 700 km further south east (Figure 1) that indicates mid Miocene temperatures of 26°C at 15.5 Ma (Leutert et al., 2020). Site 1168 SST are, on the other hand 5.5°C warmer than TEX_{86} temperatures estimates found at the Antarctic Margin (Hartman et al., 2018). Our estimation of colder early Miocene temperatures are consistent with terrestrial indicators suggesting a landscape similar to the modern tundra in the continent (DSDP 270; also seen at CRP-2 Kulhanek et al. (2019)); marine records suggest and lower SST in the area and a distal ice sheet grounding-line.

5.3 Evolution of temperature gradients in the Southern Ocean

Because in the Oligocene- - Early Miocene global ice volume was concentrated in Antarctica, and because deep-water formation is interpreted to have occurred in the Southern Ocean, the evolution of SST in the Southern Ocean is of particular relevance to interpretations of the benthic $\delta^{18}O$ and its potential ice volume and deep ocean temperature components. It is widely assumed that ice volume is coupled to deep-water temperatures, but recent model simulations suggest that this relationship is nonlinear and that there may be very limited changes in deep-water temperature when Antarctic ice sheet height but not aerial extent varies (Bradshaw et al., 2021). If the 3°C warming of SST estimated from the Site 1168 temperature anomaly over the LOW was broadly representative of temperature trends elsewhere in the Southern Ocean, including regions of deep-water formation, this would suggest that the ~27 to 24 Ma trend in benthic $\delta^{18}O$ marking the LOW could have a significant deep ocean temperature component. However, deep-water temperatures estimated from the Mg/Ca of benthic foraminifer in deep Pacific sites (Cramer et al., 2011; Lear et al., 2004) suggest negligible temperature change across over this time interval. If this deep-water temperature trend is not affected by uncertainties in the benthic Mg/Ca calibration and effect of secondary influences (Hollis et al., 2019), it suggests a large decrease in ice volume responsible for the benthic $\delta^{18}O$ shift over the LOW.

If bottom water temperatures did not change through the LOW, then the warming at Site 1168 suggests an increasing latitudinal temperature gradient between the Antarctic margin site of deep-water formation and the Tasmanian Rise. Indeed GDGTs-derived SST on the Wilkes Land Antarctic Margin Site 1356 over this interval (consistently at 60°S, Figure 1 Map (Torsvik et al., 2012; van Hinsbergen et al., 2015)) also show no evidence of warming through the Late Oligocene (Hartman et al., 2018; Salabarnada et al., 2018) (Figure 5). If TEX_{86} at Wilkes land margin accurately records changes in SST during this time period without bias from reworking (Bijl et al., 2018; Hartman et al., 2018; Hoem et al., 2020) the data imply an increasing thermal gradient between Site 1168 and the Wilkes land margin (Figure 5). Potentially, the final opening of the Tasmanian Gateway by 27.5 Ma caused in the alignment of the westerlies winds with the Drake passage and a gradual strengthening of the proto-ACC (Exon et al., 2001; Nicholson and Stow, 2019; Pfuhl and McCave, 2005; Pfuhl et al., 2004; Scher et al., 2015) reducing the poleward heat transport towards the Wilkes Land Antarctic margin. However, this interpretation of increasing thermal isolation of Antarctica resulting in constant deepwater temperatures would then require additional mechanisms other than proximal ocean warmth to trigger the hypothesized decrease in Antarctic ice volume during the LOW. Furthermore, the absence of deep-water temperature change would imply the LOW was characterized by primarily by a reduction in Antarctic ice sheet height. In the absence of proximal ocean warming, one mechanism to trigger ice retreat might be greenhouse forcing, however ε_p-based proxy long term estimates suggest decreasing or stable CO_2 through the LOW (Zhang et al., 2013).

Alternatively, GDGT-based SST estimates in the North Atlantic do not resolve warming trends that are resolved by alkenone-based SST (Guitián et al., 2019). If this is true on the Wilkes margin, then the potential for broad Southern Ocean warming may need to be further explored. Given uncertainties in both deep-water and SST proxies, additional temperature records at different latitudes in the Southern Ocean at this time would be useful to distinguish the spatial extent of Southern Ocean warming during the LOW and the nature and cause of any ice volume changes at this time.

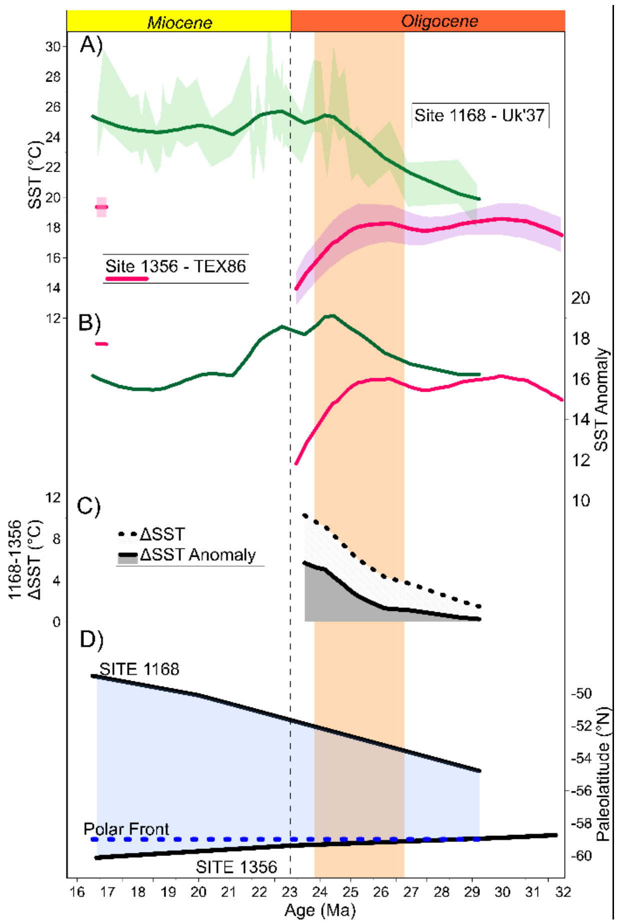

Figure 5. (**a**) SST reconstructions from $U^{k'}_{37}$ ODP 1168 and TEX$_{86}$ ODP 1356 (Hartman et al., 2018). (**b**) Reconstructed SST anomaly for both sites. (**c**) Temperature gradient between ODP

1168 and ODP 1356. (**d**) Paleolatitude estimations for both sites ODP 1356 (Torsvik et al., 2012; van Hinsbergen et al., 2015) and estimated position of the PF between the two sites (Salabarnada et al., 2018; Scher et al., 2015) using same paleolatitude reconstruction frame.

5.4 Late Oligocene Warming magnitude in the Southern and Northern Hemisphere

Although there are hiatuses during the MOGI in mid-latitude Northern hemisphere sites, alkenone-derived SST suggest similar magnitude warming as Site 1168 (Figure 6). Our Southern Ocean inference of 4°C of SST-anomaly from 29 Ma to the stabilization at 24.5 Ma is similar to ca 3°C warmer Late Oligocene than the preceeding Early Oligocene inferred from alkenone-derived temperatures from 40°N Atlantic Site 1406 (Guitián et al., 2019). Likewise, at nearby IODP Site 1404 SST increases by 4°C from 26.8 to 23.5 Ma. a (Liu et al., 2018).

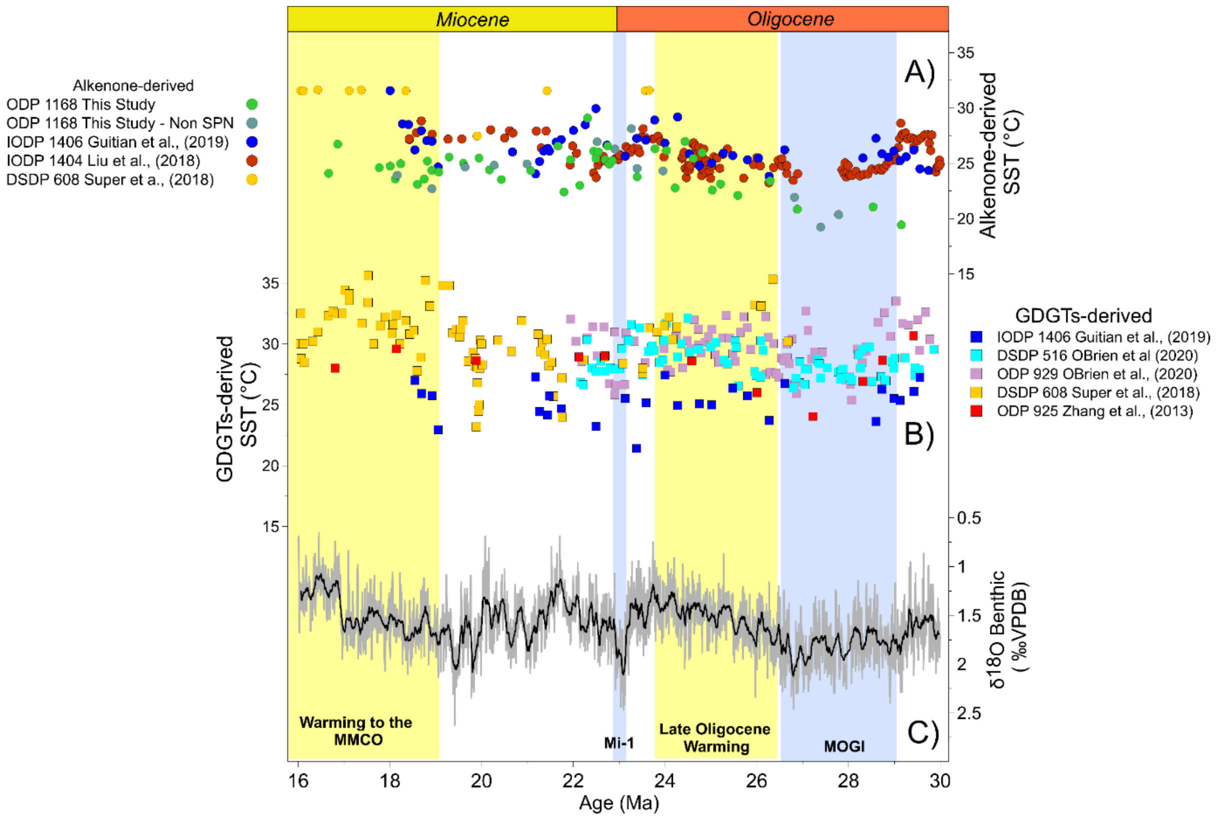

Figure 6. Oligocene to Miocene long-term SST records from low to mid latitude sites classified by proxy. (**a**) Alkenone-derived SST calibrated from the $U^{k\prime}_{37}$ ratio with BAYSPLINE (Tierney and Tingley, 2018). (**b**) GDGTs-derived SST from TEX_{86} using BAYSPARE calibration (Tierney and Tingley, 2015). Note that SST records are presented without adjustment for latitudinal shift at any site as it is likely that only Site 1168 present significant anomaly. Both SST axis show equivalent magnitude. Vertical yellow and blue bands show main warming and cold period discussed in the text. (**c**) Benthic reference megasplice (De Vleeschouwer et al., 2017).

The LOW has been more difficult to distinguish in GDGT-derived SST estimates. Northern Hemisphere GDGT-derived records from mid-latitude Sites DSDP 608 and IODP Site 1406, do not support any warming across the Late Oligocene (Guitián et al., 2019; Super et al., 2018) despite similar latitude to our Southern Hemisphere Site 1168 record. Only southern mid-latitude Atlantic Site 516 GDGTs-reconstructions identify a clear increase of the mean temperature coincident with Site 1168 alkenone-derived SST from 27.5 to 24 Ma, but this is a modest change of only 1.5°C and no lower temperature sampled earlier in the middle Oligocene (O'Brien et al., 2020). High resolution (100ky) GDGTs reconstructions at Equatorial Atlantic ODP Site 929 show no evident warming over the entire Late Oligocene –Miocene, and if there is one, appear to be only 2.5°C from 26.5 Ma to 25.5 Ma (O'Brien et al., 2020). Because the $U_{37}^{k\prime}$ ratio is saturated in most tropical sites, estimations of polar amplification at the moment rely on comparison of low latitude GDGT-based SST records with the higher latitude alkenone-based records, potentially conflating proxy-specific effects with true variations in the latitudinal expression of the Late Oligocene climate changes.

6. Conclusions

The Tasmanian Sea ODP Site 1168 alkenone-derived SST record shows for the first time cold conditions related with the MOGI, and confirms in the Southern Hemisphere, the previously recognized subsequent long-term warming through the Late Oligocene. By 29 Ma, 20°C, SST characterized the middle Oligocene at Site 1168. A subsequent 5°C increase in SST between 27 and 24.5 Ma coincided with the end the MOGI. Apparent warmer temperatures exist during the latest Oligocene and transition to the Miocene around 24.5-22.5°C, cooling down 2°C to finally stabilize into the Miocene around 20.1 Ma, although the Oligocene Miocene transition might not be sampled here. The variability of SST is higher in the warm Late Oligocene and more stable in the relatively colder Early Miocene. Reconstructed latitudinal drift of the site does not explain the observed long-term temperature trends. Calculated true temperature anomalies for a given latitude still document a significant late Oligocene SST increase. Comparison with previously published records from the Atlantic Ocean and surrounding Antarctic locations, highlights the discrepancy in warming amplitude among records from differing proxies and locations and underscores the need for further evaluation of proxies and oceanic circulation to provide a coherent picture of Southern Ocean climate evolution through the Oligocene to early Miocene.

7. Acknowledgments and Data

Sediment samples were provided by the Ocean Drilling Program (ODP). This study was supported by the Swiss National Science Foundation (Award 200021_182070 to Heather Stoll). Authors are very thankful to Madalina Jaggi, Stewart Bishop, and Thierry Solms for assistance in the laboratory. We also thank Lena Thöle and Mariska Hoorweg for providing the subset of samples from Utrecht University with an ERC starting grant n802835 OceaNice to Peter K. Bijl. Data generated for this work is uploaded as independent excel file as Supplementary Information Table S2 and archived online at Zenodo Data Archive (link will be provided once manuscript is accepted).

8. References

Bijl, P.K., Houben, A.J., Hartman, J.D., Pross, J., Salabarnada, A., Escutia, C., Sangiorgi, F., 2018. Paleoceanography and ice sheet variability offshore Wilkes Land, Antarctica-Part 2: Insights from Oligocene-Miocene dinoflagellate cyst assemblages. Climate of the Past 14, 1015-1033.

Bradshaw, C.D., Langebroek, P.M., Lear, C.H., Lunt, D.J., Coxall, H.K., Sosdian, S.M., de Boer, A.M., 2021. Hydrological impact of Middle Miocene Antarctic ice-free areas coupled to deep ocean temperatures. Nature Geoscience 14, 429-436.

Brassell, S., Eglinton, G., Marlowe, I., Pflaumann, U., Sarnthein, M., 1986. Molecular stratigraphy: a new tool for climatic assessment. Nature 320, 129.

Brassell, S.C., 1993. Applications of biomarkers for delineating marine paleoclimatic fluctuations during the Pleistocene, Organic Geochemistry. Springer, pp. 699-738.

Conte, M.H., Eglinton, G., 1993. Alkenone and alkenoate distributions within the euphotic zone of the eastern North Atlantic: correlation with production temperature. Deep Sea Research Part I: Oceanographic Research Papers 40, 1935-1961.

Conte, M.H., Sicre, M.A., Rühlemann, C., Weber, J.C., Schulte, S., Schulz-Bull, D., Blanz, T., 2006. Global temperature calibration of the alkenone unsaturation index (UK′ 37) in surface waters and comparison with surface sediments. Geochemistry, Geophysics, Geosystems 7.

Conte, M.H., Thompson, A., Lesley, D., Harris, R.P., 1998. Genetic and physiological influences on the alkenone/alkenoate versus growth temperature relationship in Emiliania huxleyi and Gephyrocapsa oceanica. Geochimica et Cosmochimica Acta 62, 51-68.

Cramer, B., Miller, K., Barrett, P., Wright, J., 2011. Late Cretaceous–Neogene trends in deep ocean temperature and continental ice volume: Reconciling records of benthic foraminiferal geochemistry (δ18O and Mg/Ca) with sea level history. Journal of Geophysical Research: Oceans 116.

D'Andrea, W.J., Theroux, S., Bradley, R.S., Huang, X., 2016. Does phylogeny control U37K-temperature sensitivity? Implications for lacustrine alkenone paleothermometry. Geochimica et Cosmochimica Acta 175, 168-180.

De Vleeschouwer, D., Vahlenkamp, M., Crucifix, M., Pälike, H., 2017. Alternating Southern and Northern Hemisphere climate response to astronomical forcing during the past 35 my. Geology 45, 375-378.

Exon, N., Kennett, J., Malone, M., 2001. 1. LEG 189 SUMMARY, Proceedings of the Ocean Drilling Program.

Exon, N., Kennett, J., Malone, M., Brinkhuis, H., Chaproniere, G., Ennyu, A., Fothergill, P., Fuller, M., Grauert, M., Hill, P., 2002. Drilling reveals climatic consequences of Tasmanian Gateway opening. Eos, Transactions American Geophysical Union 83, 253-259.

Gong, C., Hollander, D.J., 1999. Evidence for differential degradation of alkenones under contrasting bottom water oxygen conditions: Implication for paleotemperature reconstruction. Geochimica et Cosmochimica Acta 63, 405-411.

Gradstein, F.M., Ogg, J.G., Schmitz, M., Ogg, G., 2012. The geologic time scale 2012. elsevier.

Grimalt, J.O., Rullkötter, J., Sicre, M.A., Summons, R., Farrington, J., Harvey, H.R., Goñi, M., Sawada, K., 2000. Modifications of the C37 alkenone and alkenoate composition in the water column and sediment: Possible implications for sea surface temperature estimates in paleoceanography. Geochemistry, Geophysics, Geosystems 1.

Guitián, J., Dunkley Jones, T., Hernández-Almeida, I., Löffel, T., Stoll, H.M., 2020. Adaptations of coccolithophore size to selective pressures during the Oligocene - Early Miocene high CO2 world. Paleoceanography and Paleoclimatology n/a, e2020PA003918.

Guitián, J., Phelps, S., Polissar, P.J., Ausín, B., Eglinton, T.I., Stoll, H.M., 2019. Midlatitude Temperature Variations in the Oligocene to Early Miocene. Paleoceanography and Paleoclimatology 34, 1328-1343.

Hartman, J.D., Sangiorgi, F., Escutia Dotti, C., 2018. Paleoceanography and ice sheet variability offshore Wilkes Land, Antarctica–Part 3: Insights from Oligocene–Miocene TEX86-based sea surface temperature reconstructions.

Herbert, T.D., Lawrence, K.T., Tzanova, A., Peterson, L.C., Caballero-Gill, R., Kelly, C.S., 2016. Late Miocene global cooling and the rise of modern ecosystems. Nature Geoscience 9, 843.

Hill, P.J., Exon, N.F., 2004. Tectonics and basin development of the offshore Tasmanian area incorporating results from deep ocean drilling. GMS 151, 19-42.

Hochmuth, K., Gohl, K., Leitchenkov, G., Sauermilch, I., Whittaker, J.M., Uenzelmann-Neben, G., Davy, B., De Santis, L., 2020. The evolving paleobathymetry of the circum-Antarctic Southern Ocean since 34 Ma: A key to understanding past cryosphere-ocean developments. Geochemistry, Geophysics, Geosystems 21, e2020GC009122.

Hoem, F.S., Valero, L., Evangelinos, D., Escutia, C., Duncan, B., McKay, R.M., Brinkhuis, H., Sangiorgi, F., Bijl, P.K., 2020. Temperate Oligocene surface ocean conditions offshore Cape Adare, Ross Sea, Antarctica. Climate of the Past Discussions, 1-32.

Hollis, C.J., Dunkley Jones, T., Anagnostou, E., Bijl, P.K., Cramwinckel, M.J., Cui, Y., Dickens, G.R., Edgar, K.M., Eley, Y., Evans, D., 2019. The DeepMIP contribution to PMIP4: methodologies for selection, compilation and analysis of latest Paleocene and early Eocene climate proxy data, incorporating version 0.1 of the DeepMIP database. Geoscientific Model Development 12, 3149-3206.

Houben, A.J., Bijl, P.K., Sluijs, A., Schouten, S., Brinkhuis, H., 2019. Late Eocene Southern Ocean cooling and invigoration of circulation preconditioned Antarctica for full-scale glaciation. Geochemistry, Geophysics, Geosystems 20, 2214-2234.

Kaiser, J., van der Meer, M.T., Arz, H.W., 2017. Long-chain alkenones in Baltic Sea surface sediments: new insights. Organic Geochemistry 112, 93-104.

Kennedy-Asser, A.T., Lunt, D.J., Valdes, P.J., Ladant, J.-B., Frieling, J., Lauretano, V., 2020. Changes in the high-latitude Southern Hemisphere through the Eocene–Oligocene transition: a model–data comparison. Climate of the Past 16.

Kulhanek, D.K., Levy, R.H., Clowes, C.D., Prebble, J.G., Rodelli, D., Jovane, L., Morgans, H.E., Kraus, C., Zwingmann, H., Griffith, E.M., 2019. Revised chronostratigraphy of DSDP Site 270 and late Oligocene to early Miocene paleoecology of the Ross Sea sector of Antarctica. Global and Planetary Change 178, 46-64.

Lear, C.H., Rosenthal, Y., Coxall, H.K., Wilson, P., 2004. Late Eocene to early Miocene ice sheet dynamics and the global carbon cycle. Paleoceanography 19.

Leutert, T.J., Auderset, A., Martínez-García, A., Modestou, S., Meckler, A.N., 2020. Coupled Southern Ocean cooling and Antarctic ice sheet expansion during the middle Miocene. Nature Geoscience 13, 634-639.

Liebrand, D., de Bakker, A.T., Beddow, H.M., Wilson, P.A., Bohaty, S.M., Ruessink, G., Palike, H., Batenburg, S.J., Hilgen, F.J., Hodell, D.A., Huck, C.E., Kroon, D., Raffi, I., Saes, M.J., van Dijk, A.E., Lourens, L.J., 2017. Evolution of the early Antarctic ice ages. Proc Natl Acad Sci U S A 114, 3867-3872.

Liu, Z., He, Y., Jiang, Y., Wang, H., Liu, W., Bohaty, S.M., Wilson, P.A., 2018. Transient temperature asymmetry between hemispheres in the Palaeogene Atlantic Ocean. Nature Geoscience 11, 656.

Liu, Z., Pagani, M., Zinniker, D., Deconto, R., Huber, M., Brinkhuis, H., Shah, S.R., Leckie, R.M., Pearson, A., 2009. Global cooling during the eocene-oligocene climate transition. Science 323, 1187-1190.

Locarnini, R., Mishonov, A., Antonov, J., Boyer, T., Garcia, H., Baranova, O., Zweng, M., Paver, C., Reagan, J., Johnson, D., 2013. World Ocean Atlas 2013, Volume 1: Temperature, edited by: Levitus, S. A. Mishonov Technical Ed., NOAA Atlas NESDIS 73, 40.

Longo, W.M., Dillon, J.T., Tarozo, R., Salacup, J.M., Huang, Y., 2013. Unprecedented separation of long chain alkenones from gas chromatography with a poly (trifluoropropylmethylsiloxane) stationary phase. Organic Geochemistry 65, 94-102.

Longo, W.M., Theroux, S., Giblin, A.E., Zheng, Y., Dillon, J.T., Huang, Y., 2016. Temperature calibration and phylogenetically distinct distributions for freshwater alkenones: Evidence from northern Alaskan lakes. Geochimica et Cosmochimica Acta 180, 177-196.

Lopez, J.F., de Oteyza, T.G., Teixidor, P., Grimalt, J.O., 2005. Long chain alkenones in hypersaline and marine coastal microbial mats. Organic Geochemistry 36, 861-872.

Marlowe, I., Brassell, S., Eglinton, G., Green, J., 1990. Long-chain alkenones and alkyl alkenoates and the fossil coccolith record of marine sediments. Chemical Geology 88, 349-375.

Mcgonigal, K.L., 2004. Quantitative Miocene calcareous nannofossil biostratigraphy from the Tasmanian Gateway. GMS 151, 191-213.

Miller, K.G., Browning, J.V., Schmelz, W.J., Kopp, R.E., Mountain, G.S., Wright, J.D., 2020. Cenozoic sea-level and cryospheric evolution from deep-sea geochemical and continental margin records. Science advances 6, eaaz1346.

Müller, P.J., Kirst, G., Ruhland, G., Von Storch, I., Rosell-Melé, A., 1998. Calibration of the alkenone paleotemperature index U37K′ based on core-tops from the eastern South Atlantic and the global ocean (60° N-60° S). Geochimica et Cosmochimica Acta 62, 1757-1772.

Nicholson, U., Stow, D., 2019. Erosion and deposition beneath the Subantarctic Front since the Early Oligocene. Scientific reports 9, 1-9.

O'Neill, C., Müller, D., Steinberger, B., 2005. On the uncertainties in hot spot reconstructions and the significance of moving hot spot reference frames. Geochemistry, Geophysics, Geosystems 6.

O’Brien, C.L., Huber, M., Thomas, E., Pagani, M., Super, J.R., Elder, L.E., Hull, P.M., 2020. The enigma of Oligocene climate and global surface temperature evolution. Proceedings of the National Academy of Sciences 117, 25302-25309.

Pälike, H., Norris, R.D., Herrle, J.O., Wilson, P.A., Coxall, H.K., Lear, C.H., Shackleton, N.J., Tripati, A.K., Wade, B.S., 2006. The heartbeat of the Oligocene climate system. science 314, 1894-1898.

Pekar, S.F., DeConto, R.M., 2006. High-resolution ice-volume estimates for the early Miocene: Evidence for a dynamic ice sheet in Antarctica. Palaeogeography, Palaeoclimatology, Palaeoecology 231, 101-109.

Pekar, S.F., DeConto, R.M., Harwood, D.M., 2006. Resolving a late Oligocene conundrum: deep-sea warming and Antarctic glaciation. Palaeogeography, Palaeoclimatology, Palaeoecology 231, 29-40.

Pfuhl, H.A., McCave, I.N., 2003. Integrated age models for the early Oligocene-early Miocene, sites 1168 and 1170–1172, Proc. ODP, Sci. Results, pp. 1-21.

Pfuhl, H.A., McCave, I.N., 2005. Evidence for late Oligocene establishment of the Antarctic Circumpolar Current. Earth and Planetary Science Letters 235, 715-728.

Pfuhl, H.A., Mccave, I.N., Schellenberg, S.A., Ferretti, P., 2004. Changes in Southern Ocean circulation in late Oligocene to early Miocene time, The Cenozoic Southern Ocean: Tectonics, Sedimentation, and Climate Change Between Australia and Antarctica. American Geophysical Union Washington/DC, pp. 173-189.

Prahl, F.G., Mix, A.C., Sparrow, M.A., 2006. Alkenone paleothermometry: Biological lessons from marine sediment records off western South America. Geochimica et Cosmochimica Acta 70, 101-117.

Prahl, F.G., Wakeham, S.G., 1987. Calibration of unsaturation patterns in long-chain ketone compositions for palaeotemperature assessment. Nature 330, 367.

Rechka, J., Maxwell, J., 1988. Unusual long chain ketones of algal origin. Tetrahedron Letters 29, 2599-2600.

Rosell-Melé, A., Carter, J., Eglinton, G., 1994. Distributions of long-chain alkenones and alkyl alkenoates in marine surface sediments from the North East Atlantic. Organic Geochemistry 22, 501-509.

Salabarnada, A., Escutia, C., Röhl, U., Nelson, C.H., McKay, R., Jiménez-Espejo, F., Bijl, P., Hartman, J., Strother, S., Salzmann, U., 2018. Paleoceanography and ice sheet variability offshore Wilkes Land, Antarctica–Part 1: Insights from late Oligocene astronomically paced contourite sedimentation. Climate of the Past 14, 991-1014.

Scher, H.D., Whittaker, J.M., Williams, S.E., Latimer, J.C., Kordesch, W.E., Delaney, M.L., 2015. Onset of Antarctic Circumpolar Current 30 million years ago as Tasmanian Gateway aligned with westerlies. Nature 523, 580-583.

Stickley, C., Brinkhuis, H., McGonigal, K., Chaproniere, G., Fuller, M., Kelly, D., Nürnberg, D., Pfuhl, H., Schellenberg, S., Schönfeld, J., 2004a. Late Cretaceous–Quaternary biomagnetostratigraphy of ODP Sites 1168, 1170, 1171, and 1172, Tasmanian Gateway, Proceedings of the Ocean Drilling Program, Scientific Results. Ocean Drilling Program, College Station TX, pp. 1-57.

Stickley, C.E., Brinkhuis, H., Schellenberg, S.A., Sluijs, A., Röhl, U., Fuller, M., Grauert, M., Huber, M., Warnaar, J., Williams, G.L., 2004b. Timing and nature of the deepening of the Tasmanian Gateway. Paleoceanography 19.

Super, J.R., Thomas, E., Pagani, M., Huber, M., O'Brien, C., Hull, P.M., 2018. North Atlantic temperature and p CO2 coupling in the early-middle Miocene. Geology 46, 519-522.

Theroux, S., D'Andrea, W.J., Toney, J., Amaral-Zettler, L., Huang, Y., 2010. Phylogenetic diversity and evolutionary relatedness of alkenone-producing haptophyte algae in lakes: implications for continental paleotemperature reconstructions. Earth and Planetary Science Letters 300, 311-320.

Tierney, J.E., Tingley, M.P., 2015. A TEX(8)(6) surface sediment database and extended Bayesian calibration. Sci Data 2, 150029.

Tierney, J.E., Tingley, M.P., 2018. BAYSPLINE: A new calibration for the alkenone paleothermometer. Paleoceanography and Paleoclimatology 33, 281-301.

Torsvik, T.H., Steinberger, B., Cocks, L.R.M., Burke, K., 2008. Longitude: linking Earth's ancient surface to its deep interior. Earth and Planetary Science Letters 276, 273-282.

Torsvik, T.H., Van der Voo, R., Preeden, U., Mac Niocaill, C., Steinberger, B., Doubrovine, P.V., Van Hinsbergen, D.J., Domeier, M., Gaina, C., Tohver, E., 2012. Phanerozoic polar wander, palaeogeography and dynamics. Earth-Science Reviews 114, 325-368.

van Hinsbergen, D.J., de Groot, L.V., van Schaik, S.J., Spakman, W., Bijl, P.K., Sluijs, A., Langereis, C.G., Brinkhuis, H., 2015. A paleolatitude calculator for paleoclimate studies. PloS one 10.

Villa, G., Persico, D., 2006. Late Oligocene climatic changes: evidence from calcareous nannofossils at Kerguelen Plateau Site 748 (Southern Ocean). Palaeogeography, Palaeoclimatology, Palaeoecology 231, 110-119.

Volkman, J.K., Eglinton, G., CoRNER, E.D., Forsberg, T., 1980. Long-chain alkenes and alkenones in the marine coccolithophorid Emiliania huxleyi. Phytochemistry 19, 2619-2622.

Wei, W., McGonigal, K.L., Zhong, S., 2003. Data report: Paleogene calcareous nannofossil biostratigraphy of ODP Leg 189 (Australia-Antarctica gateway), Proc. ODP, Sci. Results. Ocean Drilling Program College Station, TX, p. 114.

Westerhold, T., Marwan, N., Drury, A.J., Liebrand, D., Agnini, C., Anagnostou, E., Barnet, J.S., Bohaty, S.M., De Vleeschouwer, D., Florindo, F., 2020. An astronomically dated record of Earth's climate and its predictability over the last 66 million years. Science 369, 1383-1387.

Young, J.R., 1998. Neogene nannofossils. Calcareous Nannofossil Biostratigraphy. Kluwer Academic, Dordrecht 225, 265.

Zachos, J.C., Dickens, G.R., Zeebe, R.E., 2008. An early Cenozoic perspective on greenhouse warming and carbon-cycle dynamics. Nature 451, 279-283.

Zhang, Y.G., Pagani, M., Liu, Z., Bohaty, S.M., Deconto, R., 2013. A 40-million-year history of atmospheric CO(2). Philos Trans A Math Phys Eng Sci 371, 20130096.

Zheng, Y., Heng, P., Conte, M.H., Vachula, R.S., Huang, Y., 2019. Systematic chemotaxonomic profiling and novel paleotemperature indices based on alkenones and alkenoates: Potential for disentangling mixed species input. Organic Geochemistry 128, 26-41.

Zheng, Y., Tarozo, R., Huang, Y., 2017. Optimizing chromatographic resolution for simultaneous quantification of long chain alkenones, alkenoates and their double bond positional isomers. Organic Geochemistry 111, 136-143.